CrossMark

Oxidation Kinetics and Oxide Scale Characterization of Nickel-Based Superalloy IN738LC at 900 °C

H.T. Mallikarjuna, W.F. Caley, and N.L. Richards

The high-temperature isothermal oxidation behavior of the polycrystalline nickel-based superalloy IN738LC was investigated at 900 °C in air for up to 1000 h. The results from the tests suggest that the alloy showed single-stage parabolic oxidation behavior during isothermal oxidation. The oxidized samples were characterized using SEM and SEM/EDS, and the results show that the alloy is comprised of an outer dense chromia scale with titania proving Type II oxidation behavior. In addition, the formation of a spinel composition adjacent to the external layer and a discontinuous needle-shaped alumina scale in the alloy subsurface zone were also observed. The depletion of gamma prime (γ') phase leads to a precipitate-free zone formation in the subscale zone. A JMatPro thermodynamic analysis showed that an increase in titanium content from 1 to 3.44 wt.% increased the chromium activity by 50%. Therefore, the results suggest that the presence of high amounts of titanium ($\sim$3.44 wt.%) in IN738LC increased the oxidation kinetics by increasing the chromium scale growth rate and resulting in an oxidation rate constant of 2.79×10^{-6} mg^2 cm^{-4} s^{-1}.

1. Introduction

Superalloys are used in a wide range of applications where high temperature and oxidation resistance are required, while the material must concurrently maintain its mechanical integrity and microstructure. These properties of superalloys were developed over the past 60 years for applications involving aggressive operating conditions such as those experienced by components of gas turbine engines (Ref 1). Aviation gas turbines take up to three-quarters of all applications of superalloys, the other quarter going to applications such as power generation gas turbines, the chemical industry and nuclear reactors. All these high-temperature properties are obtained through solid solution strengthening and/or by precipitation hardening (Ref 2).

In recent years, the oxidation behavior of the turbine blade materials has become one of the major life-limiting factors because the surface temperature of these blades can reach up to 1100 °C (Ref 3-5). Hence, it is very important to understand the inherent property of the material in an oxidizing environment in case of thermal barrier coating (TBC) failure (Ref 6). Mechanical properties such as fatigue resistance and thermal creep deformation resistance depend on the material composition, and the capability of the material to withstand high temperature also depends on oxide scale formation and the associated kinetics.

Generally, Ni-Cr-Al alloys exposed to a high-temperature oxidizing environment may produce a variety of oxides on the surface such as NiO, Cr_2O_3, Al_2O_3, TiO_2 and Ta_2O_5. Thermodynamically, Cr_2O_3 and Al_2O_3 are the most stable oxide phases among these oxides. Geggins and Pettit (Ref 7) have studied oxidation behavior of many Ni-Cr-Al alloys at high temperatures. The formation of an external scale, i.e., Cr_2O_3 or Al_2O_3, is dependent not only on the thermodynamic equilibrium, but also on the amount of Cr and Al present in an alloy. A spinel-type oxide layer with the composition of $Ni(Cr,Al)_2O_4$ is also one of the oxide layers which is formed just beneath the external oxide layer. The formation of the spinel layer is determined by the Al concentration, and the composition of this layer changes with the exposure duration at temperature of interest.

IN738LC is designed for service in aggressive environments; this alloy contains relatively high chromium, 16 wt.%, along with several other alloying elements such as Ti, Al and Co. In service, the chromium oxidizes to form a continuous and coherent chromia scale on an alloy surface to give maximum protection by separating the substrate from the oxidizing atmosphere (Ref 8). The aluminum content also provides significant oxidation resistance to the alloy and together with chromium give maximum protection to the alloy.

The high-temperature mechanical properties of the material will be governed by the microstructure as well as by chemical composition. IN738LC is a polycrystalline alloy with face-centered cubic (FCC) γ' precipitates in the form of $Ni_3(Al,Ti)$ which are dispersed in an austenitic matrix. The strength and oxidation resistance of the alloy depend on the volume fraction of the precipitates present in the matrix (Ref 9, 10). These γ' precipitates are a storage bank of aluminum. Therefore, an increase in the volume fraction of these precipitates increases the formation of the alumina scale which tends to decrease the oxidation rate because the diffusion of oxygen ions through the alumina scale is relatively slow (Ref 11).

The oxidation mechanism in a multicomponent system such as a nickel-based superalloy is very complex because selective

H.T. Mallikarjuna, W.F. Caley, and **N.L. Richards**, Department of Mechanical Engineering, University of Manitoba, Winnipeg, MB R3T 5V6, Canada. Contact e-mail: william.caley@umanitoba.ca.

oxidation, internal oxidation and the formation of secondary oxides such as TiO_2 are involved. The present work provides a framework for the determination of both oxidation kinetics and scale formation for IN738LC under service conditions.

2. Experimental Procedure

The specimens used in the present study were prepared from polycrystalline IN738LC (C:0.112; Si:0.004; Cr:16.02; Al:3.4; Mo:1.77; Ti:3.44; Co:8.47; W:2.58; Zr:0.028; B:0.009; Nb:0.9; Ta:1.71; Ni:bal.) (wt.%). The chemical composition of the superalloy was determined by PCC airfoils, Inc. Minerva, using inductively coupled plasma mass spectroscopy (ICP-MS). The solution-treated (1120 °C) IN738LC alloy casting was aged in a vacuum furnace at 845 °C for 24 h and furnace cooled to precipitate the γ' phase from the solid solution matrix. The fully aged/heat-treated alloy bar was machined to specimens with a size of 10 mm × 8.5 mm × 2 mm. The specimens were ground to 600-grit SiC paper, ultrasonically cleaned in acetone and dried in hot air.

The isothermal oxidation kinetics was studied in static air by means of discontinuous gravimetric analysis at 900 °C for exposure times up to 1000 h. The specimens were placed in open-glazed porcelain crucibles which were placed in a Carbolite high-temperature box furnace. After various times from 1 to 1000 h, samples were withdrawn from the isothermal oxidation test and left to cool to room temperature in air. Once cooled, the samples were weighed using an electronic scale, accurate to ± 0.0001 g and the data were normalized per unit area exposed.

The oxidized specimens were then cut, embedded in epoxy resin, ground with SiC paper and polished with 1-μm diamond suspension. Subsequent electrolytic etching in 12 ml of 70% H_3PO_4 + 40 ml of 70% HNO_3 + 48 ml of 98% H_2SO_4 solution provided a topological contrast between the γ and γ' phases. The oxidized specimens were analyzed using several different characterization techniques in order to obtain the oxide structures which formed, as well as chemical composition and microstructure. The oxide scales, precipitate-free zone (PFZ) and internal oxides were examined by optical microscopy using a Zeiss Axiovert 25 followed by scanning electron microscopy (SEM) JEOL JSM-5900LV operating at 10 keV in the secondary electron mode. The phase constitution of the oxide scales was analyzed using energy-dispersive spectrometer (EDS) with INCA X-Max, operating at 20 keV.

3. Results and Discussion

3.1 Initial Microstructure Evaluation

The optical microstructure and SEM microstructure of the IN738LC before oxidation are shown in Fig. 1. The lower magnification of age-hardened IN738LC was taken using the optical microscope is shown in Fig. 1(a), where the presence of two-phase structures, γ/γ' can be seen along with MC carbides (Fig. 1a), which is common in nickel-based superalloys. The cuboidal γ' precipitates which are obtained after the aging heat treatment are indicated in the SEM micrograph, Fig. 1(b). From Fig. 1(b), a bimodal distribution of γ' can be seen. The image analysis results from Fig. 2 show that the precipitate-hardened

superalloy contained 70 vol.% of cuboidal γ' precipitates, with majority of precipitates being less than 200 nm in diameter. The sample grain size was measured to be approximately 700 μms, and the grain boundaries are decorated with $M_{23}C_6$ carbides.

3.2 Isothermal Oxidation Kinetics

Figure 3 shows the specific mass gain per unit area as a function of oxidation time after isothermal oxidation at 900 °C for up to 1000 h in static air. The oxidation curve indicates a significant increase in mass up to 400 h, whereas later stages in oxidation duration have minimum effect on the mass gain. The kinetics of oxidation can be described by examining the rate exponent or n value, which is determined by a linear least square method using the following equation (Ref 12, 13):

$$(\Delta W/A)^n = k_p \cdot t + C \qquad (Eq\ 1)$$

where $\Delta W/A$ is the specific mass gain per unit area (mg cm^{-2}), t the oxidation duration, C a constant, and k_p is the oxidation rate constant with units of mg^2 cm^{-4} s^{-1}. The slope of specific mass gain per unit area as a function of exposure duration plot gives the k_p value.

The growth rate constant n values of 2 and 3 for square and cubic mass gains as a function of oxidation duration are shown in Fig. 4(a) and (b), respectively. It can be concluded from these figures that the oxidation behavior of IN738LC follows a square power law or parabolic rate law rather than a cubic power law because Fig. 4(b) follows a polynomial fit. By the use of a least squares analysis, Fig. 4(a), the oxidation rate constant, k_p of IN738LC at 900 °C was determined to be 2.79×10^{-6} mg^2 cm^{-4} s^{-1}; the value lies in the range of different Ni-Cr alloys (Ref 14-16). Both oxidation kinetics and the oxide scale growth in IN738LC were diffusion controlled because the value of the growth time constant or rate exponent n is 2, which is similar to several chromia-forming alloys (Ref 4, 5). Conversely, if the cubic rate law of oxidation is governing, this would indicate a grain boundary diffusion-controlled mechanism (Ref 17). In the present study, elemental diffusion has taken place from the matrix as well as from the grain boundary.

3.3 Surface Morphology of Oxidized Specimens

The back-scattered electron (BSE) surface morphologies of IN738LC after 3 and 1000 h oxidation at 900 °C in static air are shown in Fig. 5 at lower magnification (700×). It is observed from Fig. 5(a) that the surface consists of a dispersed oxide scale after 3 h of oxidation. As the oxidation duration increased to 1000 h at 900 °C, the scale formation and the growth on the surface increased as shown in Fig. 5(b).

The SEM surface morphologies and EDS elemental mapping of the IN738LC after 3-h oxidation at 900 °C in air are shown in Fig. 6. After 3 h, the surface morphology showed a discontinuity in the oxide scale formation on the surface as shown in Fig. 6(a). The EDS elemental quant mapping of the oxidized surface was generated using INCA X-Max QuantMap software, with SEM operating at 20 keV in BSE mode. The quantitative elemental maps were generated from SmartMap data using the QuantMap software application. QuantMap constructs x-ray maps by calculating the quantitative data from the spectral data stored in each pixel of the SmartMap according to the current quantitative conditions. A resolution
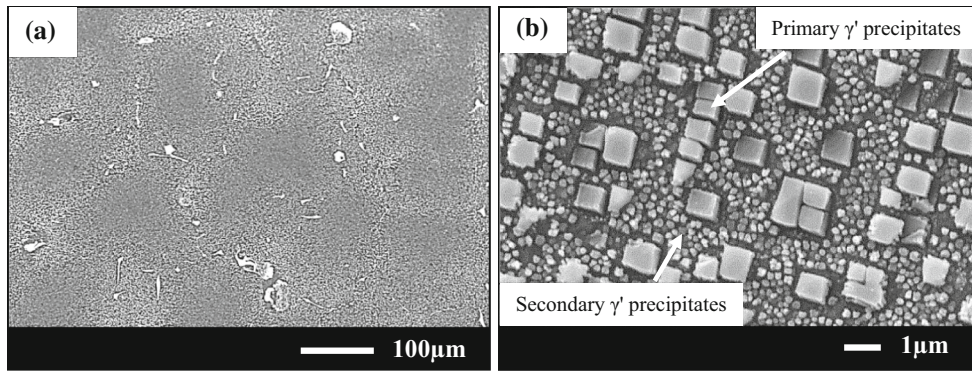
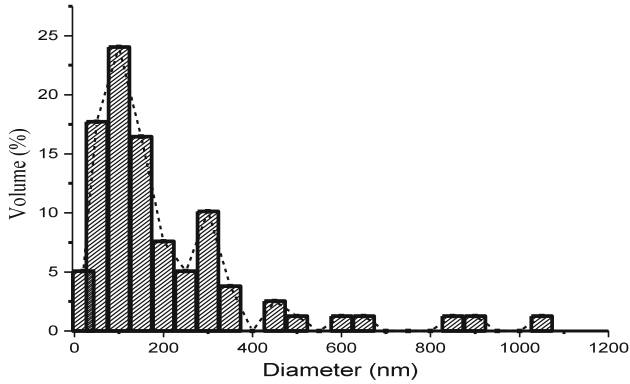**Fig. 1** (a) Optical and (b) SEM microstructure of superalloy IN738LC

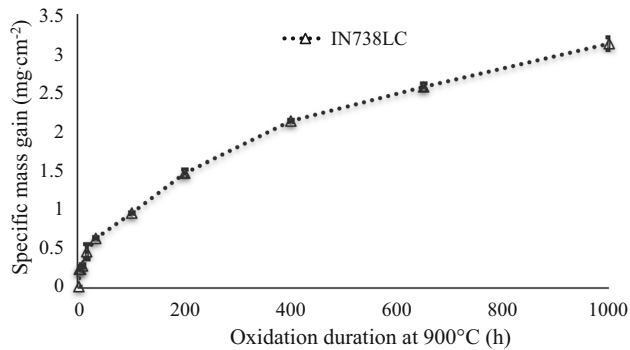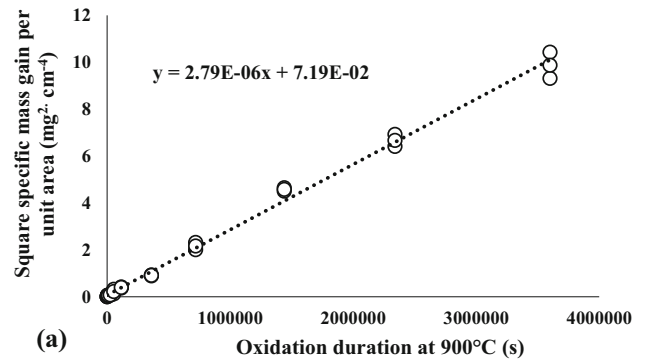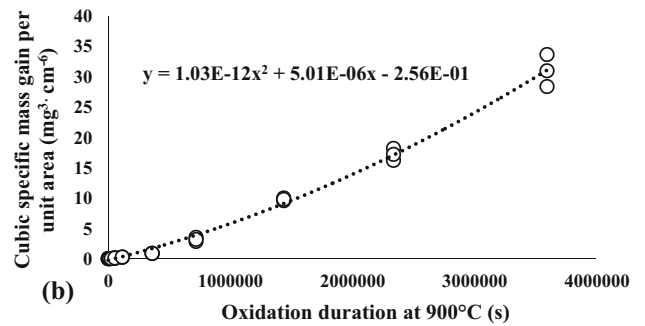**Fig. 2** Image analysis results of average γ' precipitate size as a function of volume %

Fig. 3 Specific mass gains per unit area of IN738LC at 900 °C for up to 1000 h in static air

Fig. 4 (a) Square mass gains with linear curve fitting and (b) cubic mass gains with polynomial curve fitting for IN738LC as a function of oxidation duration at 900 °C for up to 1000 h in static air

of 128×88 pixels was used for the present QuantMap created from the SmartMap data of 1024×768. The raw data from a two-dimensional (2D) EDS elemental QuantMap with the resolution of 128×88 pixels were forwarded to an Excel program, and the data were converted into three-dimensional (3D) contours using surface plot (an Excel program). These are shown in Fig. 6(b), (c), (d), (e) and (f).

The 3D schematic maps in Fig. 6 depict how each element is distributed on the alloy surface. It can be seen in Fig. 6(c), (d) and (e) that the darker regions (A) in Fig. 6(a) in the BSE image are Cr-rich and Ti-rich oxides. The brighter regions (B) in Fig. 6(a) are regions which are not oxidized after 3 h at

900 °C. The semiquantitative EDS results of the two regions (darker and brighter) in Fig. 6(a) are summarized in Table 1.

The corresponding elemental mapping results after 1000 h at 900 °C in static air are shown in Fig. 7. These data reveal that the surface of the alloy was covered with titanium-rich oxides with a small concentration of chromium-rich oxides.

The formation and development of oxides depend on the concentration of the alloying elements and thermodynamics. IN738LC is a polycrystalline alloy with grain boundaries and this could be one of the reasons for the formation of TiO_2 and Cr_2O_3 on the surface. Equilibrium thermodynamics (Ref 4) suggests that at 900 °C, TiO_2 will form first; later, chromium oxide growth will occur. Under these conditions, the rate controlling mechanism for the TiO_2 and Cr_2O_3 growth includes the migration of Ti and Cr ions from the matrix to the surface. Since diffusion of Ti and Cr is the rate controlling step, the
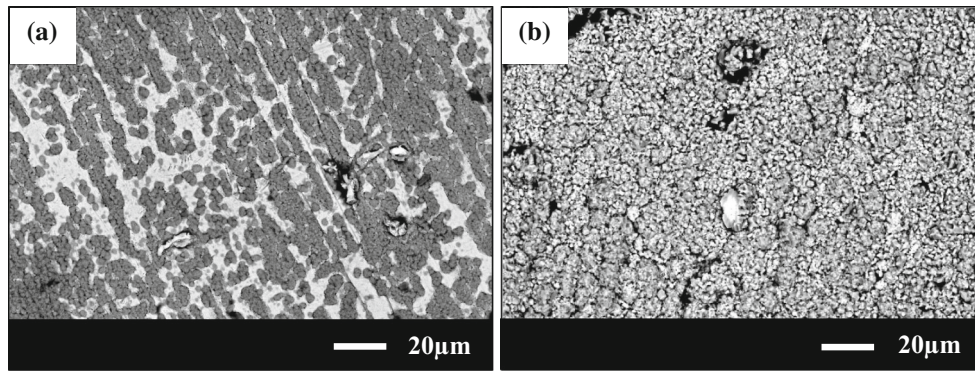
Fig. 5 BSE images of surfaces on IN738LC specimens after oxidation at 900 °C in static air (a) 3 h; (b) 1000 h
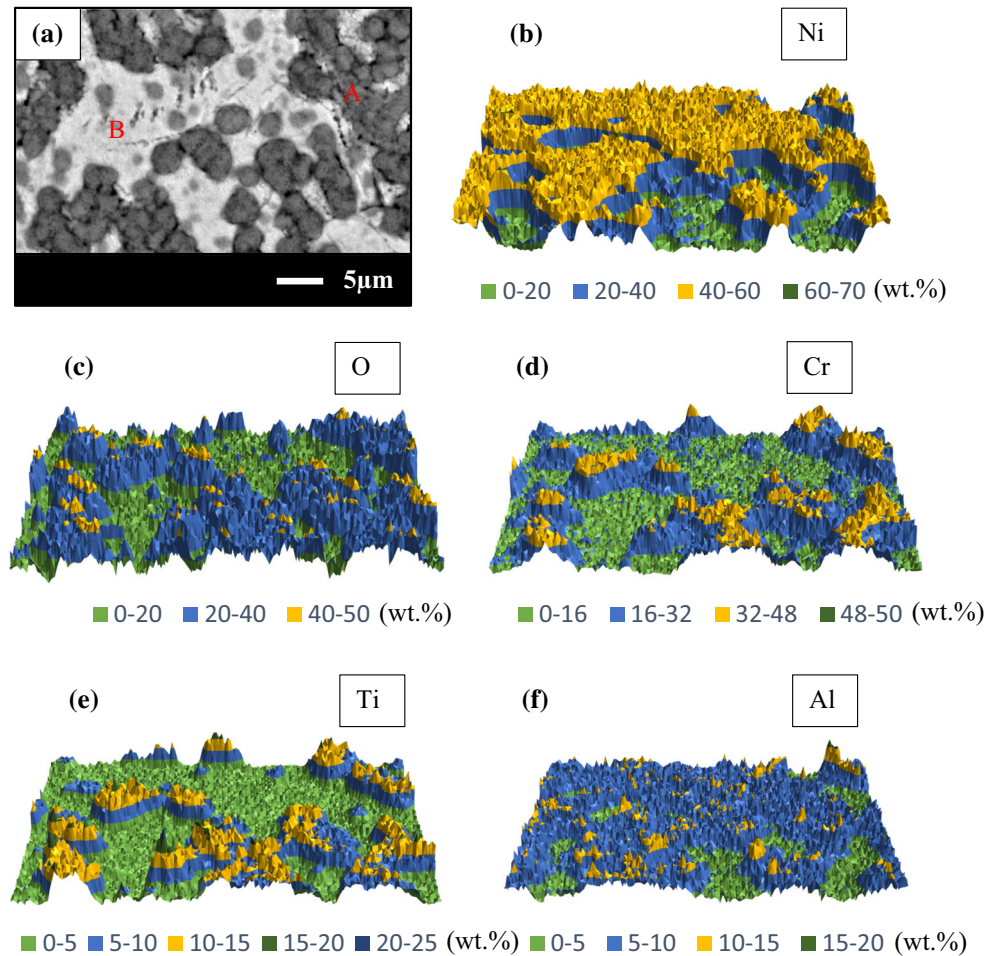

Fig. 6 (a) BSE image of IN738LC surface after 3-h oxidation at 900 °C in static air and (b), (c), (d), (e), (f) are 3D qualitative elemental maps of Ni, O, Cr, Ti, and Al, respectively

Table 1 EDS results of IN738LC after 3-h oxidation at 900 °C in static air (wt.%)

Elements	O	Al	Ti	Cr	Co	Ni	Mo	Ta	W
A, wt.%	28	6.1	8.9	25.6	3.8	22.1	0.8	2.6	2.4
B, wt.%	15	7.2	1.8	14.2	7.3	47.0	1.4	2.2	3.6

oxidation kinetics of this alloy should always show a parabolic trend.

As discussed earlier, apart from thermodynamics another factor that drives the formation of the oxide scale is the concentration/abundance of oxide-forming elements. From a
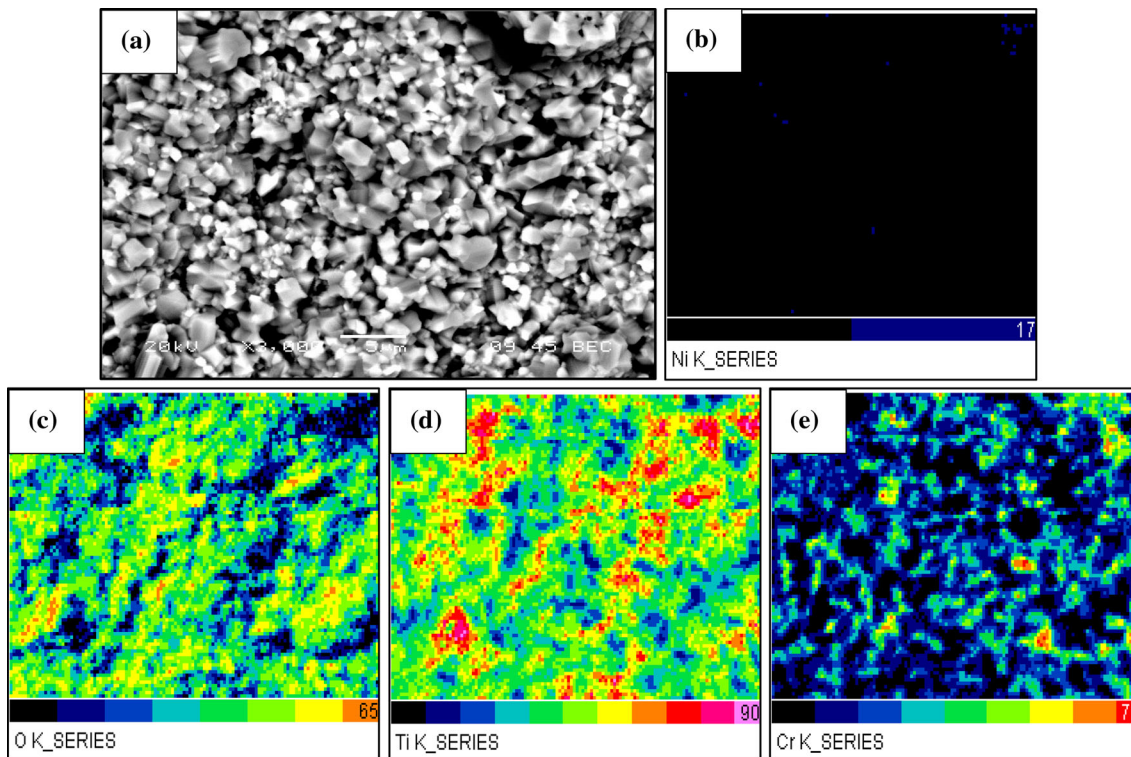
Fig. 7 BSE surface morphology and EDS elemental mapping of IN738LC after 1000-h oxidation at 900 °C in static air

Table 2 Surface EDS results of IN738LC after 1000-h oxidation at 900 °C in static air

Elements	O	Al	Ti	Cr	Co	Ni	Mo	Ta	W
Average, wt.%	33	0.1	45.5	17.8	0.4	1.3	0.5	0.6	0.7

thermodynamic point of view, TiO_2 should form preferentially to Cr_2O_3. However, the amount of titanium present in the alloy is 3.44 wt.%, whereas chromium is 16 wt.%. Therefore, TiO_2 will form only as a thin layer on the surface, as observed in the present study. The formation and growth of TiO_2 on the surface of chromium-containing alloys are possible when Ti ions diffuse through the chromium oxide scale (Ref 5). A similar mechanism was found in the present study, where Ti ions diffuse through the chromium oxide scale to form TiO_2 on the surface. However, the rate of diffusion of Ti in Cr_2O_3 appears to be slow, hence the formation of a thin TiO_2 oxide scale on the surface. The surface EDS analysis results on IN738LC after 1000 h of oxidation at 900 °C in air are summarized in Table 2.

To confirm the EDS results, specimens oxidized for 3, 15, 400 and 1000 h were subjected to x-ray diffraction analysis (XRD), as shown in Fig. 8. From Fig. 8, the 3 h specimen suggests only the formation of two oxides on the surface, namely Cr_2O_3 and TiO_2 together with the peaks corresponding to the matrix. As the oxidation duration increased, the intensities of the oxide phases increased, whereas the matrix, principally Ni-Al, decreased in intensity until 1000 h, at which point the latter has almost disappeared due to increased oxide scale thickness.
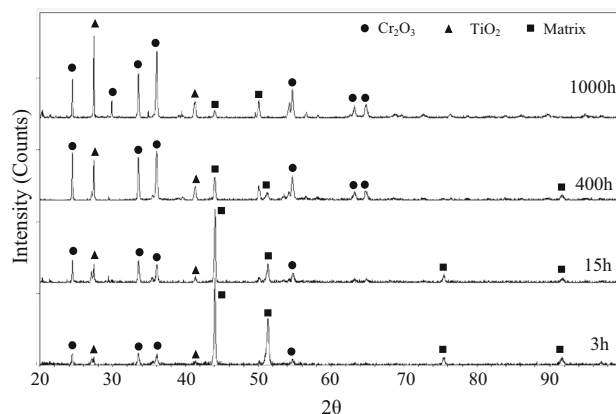

Fig. 8 X-ray diffraction spectra of IN738LC oxidized for up to 1000 h at 900 °C in static air

3.4 Cross-Sectional Characterization of the Oxidized Specimens

The cross-sectional SEM microstructure for a 3 h specimen is shown in Fig. 9 along with the line scan results. Although the oxygen activity was high enough in air to form oxides on the surface, no distinct oxide layer was identified in the cross section of this 3 h specimen. This might be due to the formation

of thin and discontinuous TiO_2 and Cr_2O_3 oxide layer formation on the surface, which could not be identified by the SEM used for this analysis. Figure 9 explains the distribution of different elements across the surface of an IN738LC specimen after 3-h oxidation at 900 °C in air. It can be seen that the surface edge in the cross-sectional region has no evidence of oxide-rich elements. However, from previous research, the growth of external oxide scale and internal oxides in the subscale regions increased gradually with the increase in the oxidation duration at high temperature (900 °C) reaching up to 10 μm thickness for the external scale and 20 μm for the internal scale including spinel and alumina (Ref 18).

Typical cross-sectional morphologies for specimens oxidized for 3-1000 h are shown in Fig. 10. Formation of internal oxides together with the surface oxides can be seen in Fig. 10(e). SEM-EDS analysis confirmed that the outer layer is Cr- and Ti-rich, and the internal finger-like structures in the subsurface zone are rich in Al. Some pores were also observed in the external Cr-rich oxide layer. It is assumed that these pores/porosity affect the solid state diffusion for the metal and oxygen ions by increasing the oxide scale growth. As shown in Fig. 7, the formation of the TiO_2 above the chromium oxide scale happened due to titanium diffusion through the chromia scale. From Fig. 10(e), the formation of internal oxides such as Al_2O_3 and the spinel composition beneath the external scale suggest that oxygen ions migrated to the subscale zones across the external Cr_2O_3 oxide scale. The depletion of γ' precipitates creates a precipitate-free zone (PFZ) in the subscale locations (Fig. 10e) due to the formation of an Al_2O_3-rich oxide scale. Thus, the $Ni_3(Al, Ti)$ precipitates act as an Al storage bank for the continuous growth of the Al_2O_3-rich oxide scale (Ref 5).

The morphology and elemental distribution of a cross-sectional specimen after 1000-h oxidation at 900 °C in static air are shown in Fig. 11. From the microstructure shown in Fig. 11(a), multiple oxide layers can be observed. The external continuous, dense and thick region is rich in chromium and oxygen as shown in Fig. 6(b) and (c), which corresponds to a Cr_2O_3 layer in Fig. 11(a), identified as a region A. Further evaluation of the EDS maps of Fig. 11(b), (c), (d), (e) and (f)

reveals that the external chromia layer consists of the measurable amount of Ti as well as a separate thin Ti-rich oxide layer on the surface. Although a thin Ti-rich layer was observed on the surface, the external scale is considered to be primarily chromia. In addition, a spinel layer with the composition of $Ni(Cr,Ti)_2O_4$ (determined using EDS line scan analysis and XRD) was observed adjacent to the external scale, which is referred as region B in Fig. 11(a). The compositional analysis of the spinel layer showed a higher amount of Cr than Ti. Since Cr occupies more lattice positions than Ti in a spinel, the amount of Ti required to form the spinel composition is relatively low (Ref 19).

The preferential oxidation of aluminum in IN738LC results in internal oxides of Al_2O_3 below the external surface and spinel layers. This Al_2O_3 has finger-like structures marked as region C in Fig. 11(a). The formation of the discontinuous oxide layer in the subsurface zone indicates poor protectiveness of external chromia layer for IN738LC. At some portions of the alloy surface, alumina has penetrated to a greater depth in the subsurface zone to the alloy grain boundaries. However, the penetration was limited to the PFZ due to the low aluminum content. The EDS analysis of the penetration region indicates the presence of titanium in the grain boundaries in the subscale region. The EDS analysis confirms that there was no oxygen associated with the titanium, but the region is rich in nitrogen indicating formation of titanium nitride. The TiN surrounding the alumina at the grain boundaries is shown in Fig. 11(d) and (e). The TiN was limited to the grain boundaries. Similar results were also found in Cruchley's work on oxidation of RR1000 over different temperatures (Ref 20).

Researchers Pettit and Meier developed a three-scale oxide scale regimes depending on their composition using a ternary alloy model such as Ni-Cr-Al (Ref 4, 7). The Type I oxidation group consists of an external NiO growth over Cr_2O_3 and Al_2O_3 oxides in the subscale region, Type II is an external Cr_2O_3 over an Al_2O_3 scale, and the third oxidation behavior is Type III, where a continuous Al_2O_3 layer is found. The present alloy falls in the Type II oxidation group, where the oxidation rate was controlled by the formation of an external Cr_2O_3 layer with internal Al_2O_3 in the subscale region.
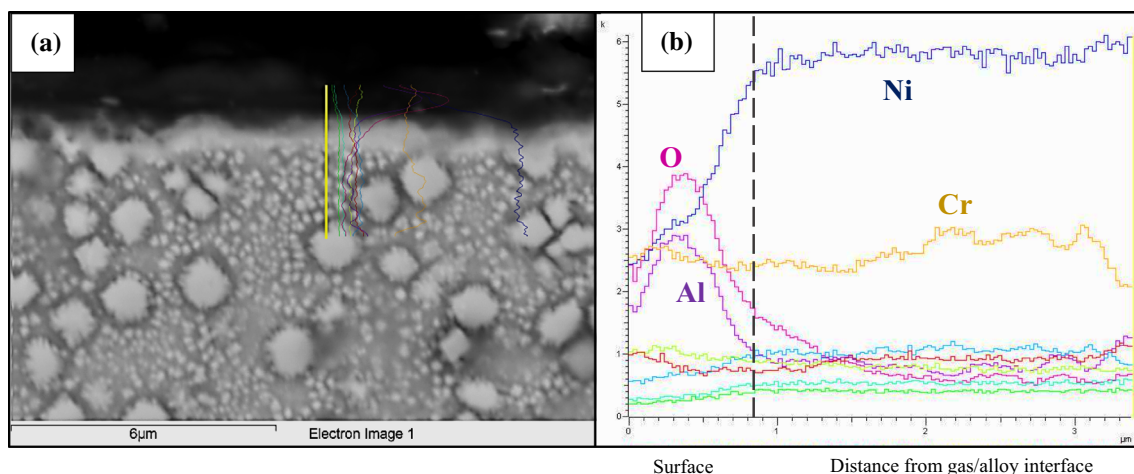

Fig. 9 Cross-sectional EDS line scan analysis of IN738LC specimen after 3-h oxidation at 900 °C in static air. (a) SEM microstructure with area of interest (b) line scan results
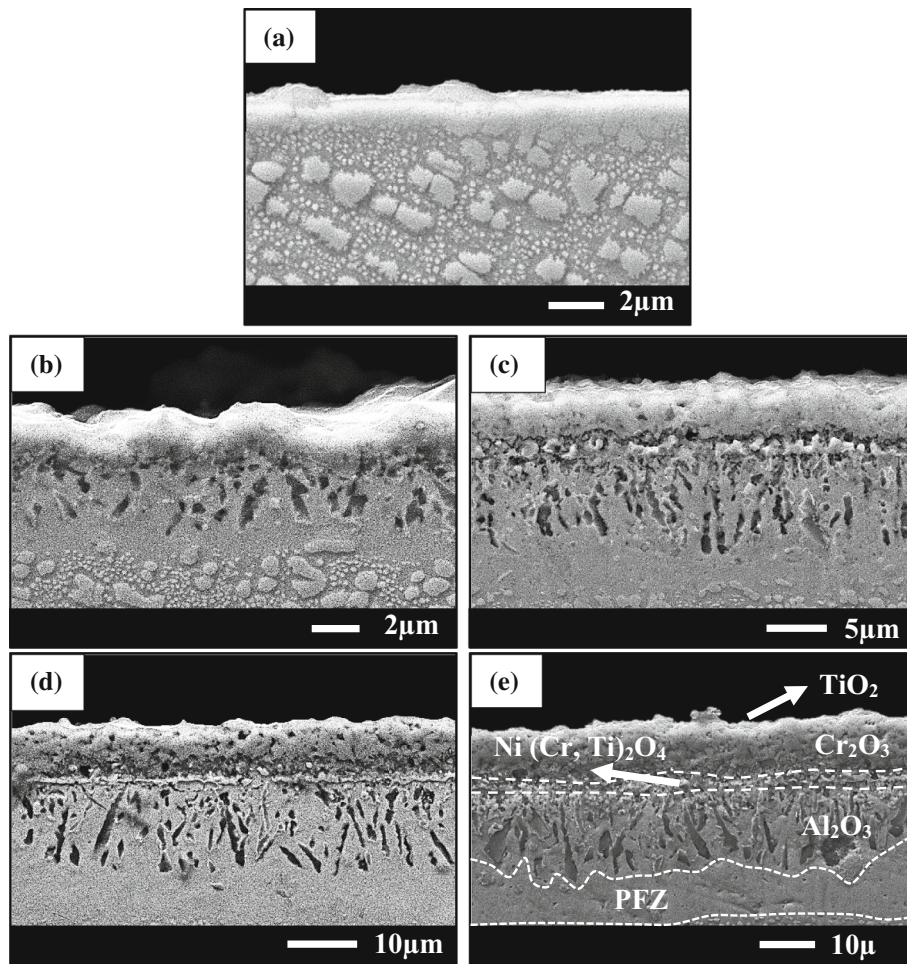
Fig. 10 SEM images of the cross section of specimens oxidized at 900 °C in static air. (a) 3 h (b) 15 h (c) 100 h (d) 400 h (e) 1000 h
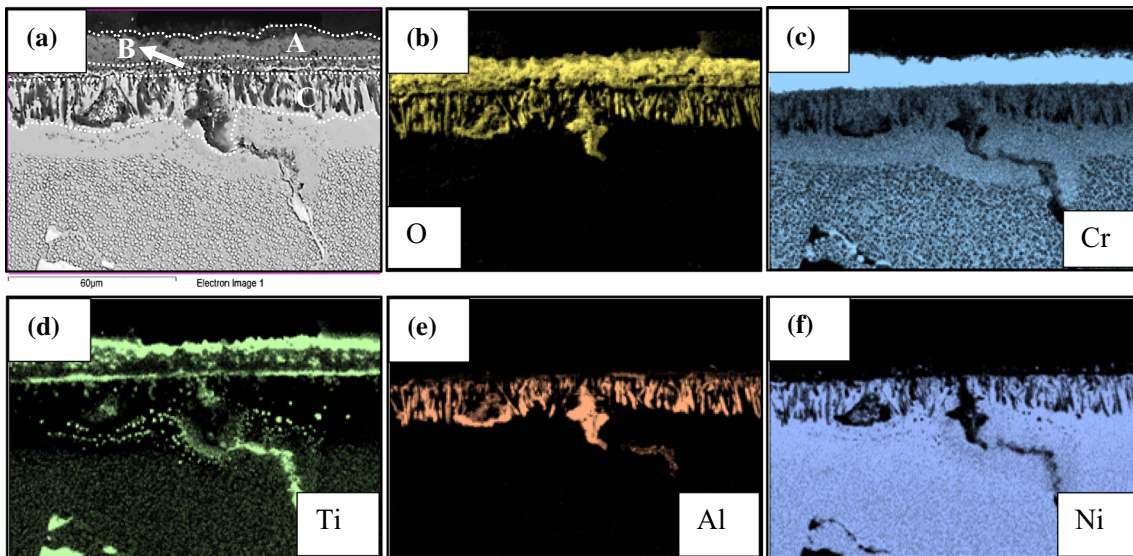

Fig. 11 Cross-sectional morphology and elemental distribution in IN738LC after oxidation for 1000 h at 900 °C in static air; (a) BSE image, (b), (c), (d), (e), (f) mapping for the elements O, Cr, Ti, Al and Ni, respectively

The Cr and Al contents of IN738LC are plotted on a Ni-Cr-Al oxidation map (Ref 21, 22), as shown in Fig. 12. The plot reveals that the alloy would be anticipated to form an Al_2O_3 scale on the surface after exposure to an oxidizing environment at 900 °C. This contradicts the findings of present work, which show that IN738LC forms a dense Cr_2O_3 scale and internal
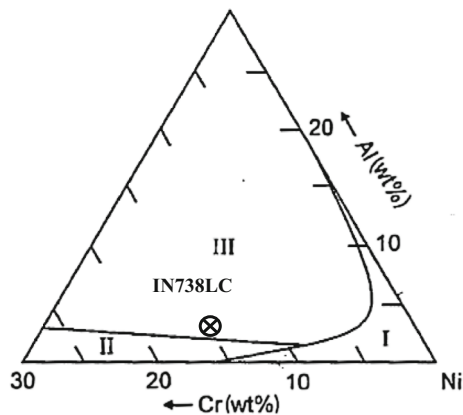
Fig. 12 Oxidation map for ternary NiCrAl alloys during isothermal oxidation in air at 1000 °C (Ref 4, 25). The Cr and Al composition of IN738LC is inserted in the oxidation map ⊗ where I, II and III are the three types of oxidation regimes (Ref 4, 21, 22)
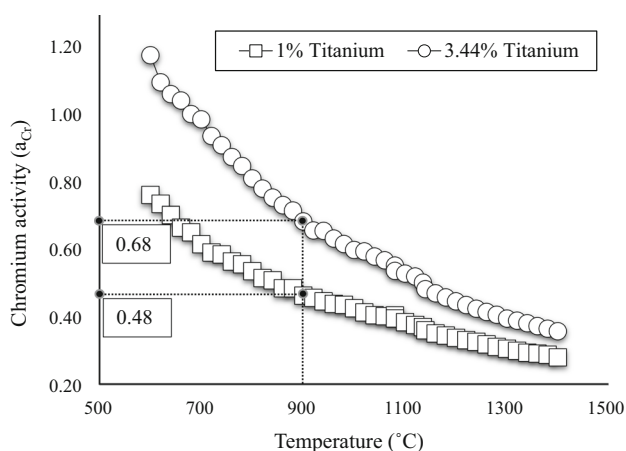

Fig. 13 JMatPro thermodynamic modeling; effect of Ti concentration on chromium activity in IN738LC at 900 °C

Al_2O_3 scale in the subsurface region. The probable reason for this deviation may be that the oxidation map shown for the ternary Ni-Cr-Al alloy was at 1000 °C and the present study was done at 900 °C. As well, the chemistry of IN738LC is considerably more complex than the simple ternary shown in Fig. 12.

At temperature ranges from 950 to 1020 °C, Cr_2O_3 will decompose to form a low-melting oxide such as CrO_3 (Ref 23). The presence of this low-melting oxide phase or liquid phase will lead to linear oxidation in the system, which will finally disintegrate the alloy. The CrO_3 is volatile at such high temperatures although its vapor pressure is low at that temperature. A similar phenomenon was also found in the low-melting oxide systems such as V_2O_5 (674 °C) and MoO_3 (795 °C) (Ref 24). Hence, alumina will form because it is the most stable oxide at this temperature.

3.5 Effect of Ti Concentration Using JMatPro

In the present work, the mechanism of the chromia scale growth rate in the presence of Ti in the IN738LC alloy was studied using the thermodynamic software JMatPro. The Ti content was varied from 1 to 3.44 wt.%, and the resulting

chromium activity was noted from the JMatPro analysis. From Fig. 13, it is evident that the chromium activity increases with an increase in the titanium content. The chromium activity (a_{Cr}) for IN738LC at 900 °C is 0.68 for 3.44 wt.% of Ti and decreased to 0.48 when the Ti concentration reduced to 1 wt.%. Therefore, the chromium is more likely to oxidize in the presence of titanium.

The decrease in the oxidation resistance of Ni-based superalloys in the presence of a wide range of Ti has been studied by a number of authors (Ref 20, 26, 27). The addition of 2 wt.% Ti has been proposed by Taniguchi et al. (Ref 28) to enhance the oxidation resistance by forming an adherent oxide scale, although grain boundary oxidation was not reported. Generally, more than 2 wt.% Ti addition revealed a precipitate lattice distortion by occupying former chromium lattice points resulting in the volume change (Ref 29). In the present case, the IN738LC alloy contains 3.44 wt.% Ti which explains the increase in the oxide scale growth. The higher chromia growth rate of IN738LC could be related to the incorporation of Ti in the oxide scale. The presence of higher amount Ti creates vacancies in the scale by replacing Cr^{3+} with Ti^{4+} ions. Hence, the concentration of Cr vacancies increases in the chromia scale (Ref 30, 31) as follows:

$$3TiO_2(+Cr_2O_3) \rightarrow 3Ti_{Cr}^* + V_{Cr}''' + 6O_o^x(+Cr_2O_3) \qquad \text{(Eq 2)}$$
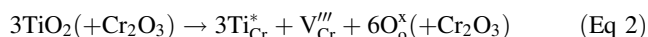
where the triple-charged chromium vacancy is given by V_{Cr}''', and the oxygen ion on oxygen sub-lattice is denoted by O_o^x. The presence of the titanium ions on chromium lattice sites (Ti_{Cr}^*) increases the positive charge, which is represented in Eq 2 (right side).

4. Conclusions

An isothermal oxidation study has been conducted on polycrystalline nickel-based superalloy IN738LC at 900 °C for up to 1000 h and oxidation kinetics, microstructure, the evolution of different phases and chemical composition were systematically investigated. The following conclusions are drawn:

The alloy showed Type II oxidation behavior with a chromia layer outside and alumina scale in the subsurface zone. The rate and the scale growth both followed parabolic oxidation kinetics. The rate constant was calculated to be 2.79×10^{-6} mg^2 cm^{-4} s^{-1}.

The alloy exhibited a thick chromia scale covered with a thin TiO_2 scale after 1000 h exposure at 900 °C in air. The subscale region had an internal alumina layer with many protrusions, and basically, TiO_2 encapsulated Al_2O_3 and these were limited to the PFZ.

The rapid growth of a chromia scale on the IN738LC alloy was attributed to the addition of 3.44 wt.% Ti, which increased the growth rate of the Cr_2O_3 scale by injecting vacancies in the chromia scale, thereby decreasing the likelihood of formation of a protective Al_2O_3 scale. Chromium activity increases with an increase in Ti, as confirmed by thermodynamic modeling using JMatPro software.

References

1. R.C. Reed, *The Superalloys: Fundamentals and Applications*, Cambridge University Press, Cambridge, 2006
2. A. Thakur, *Microstructural Responses of a Nickel-Base Cast IN-738 Superalloy to a Variety of Pre-weld Heat-Treatments*. M.Sc., University of Manitoba (1997)
3. R.C. Reed et al., Oxidation and Coating Evolution in Aluminized Fourth Generation Blade, in *The Minerals, Metals & Materials Society*, pp. 661–670 (2008)
4. N. Birks, G.H. Meier, and F.S. Pettit, *Introduction to the High-Temperature Oxidation of Metals*, Cambridge University Press, Cambridge, 2006
5. D.J. Young, *High Temperature Oxidation and Corrosion of Metals*, Elsevier, Oxford, 2008
6. F.A. Perez-Gonzalez, N.F. Garza-Montes-de Oca, and R. Colas, High Temperature Oxidation of the Haynes 282© Nickel-Based Superalloy, *Oxid. Met.*, 2014, **82**, p 145–161
7. C.S. Giggins and F.S. Pettit, Oxidation of Ni-Cr-Al Alloys Between 1000 and 1200 °C, *J. Electrochem. Soc.*, 1971, **118**, p 1782
8. B. Gleeson, The Long-Term, Cyclic-Oxidation Behavior of Selected Chromia-Forming Alloys, *Oxid. Met.*, 1998, **49**, p 373–399
9. M.J. Donachie and S. Donachie, *Superalloys: A Technical Guide*, ASM International, Materials Park, 2002
10. J.L. Smialek and G.H. Meier, *Superalloys II*, Wiley, New York, 1987
11. D.J. Young, A. Chyrkin, and W.J. Quadakkers, A Simple Expression for Predicting the Oxidation Limited Life of Thin Components Manufactured from FCC High Temperature Alloys, *Oxid. Met.*, 2012, **77**, p 253–264
12. N.B. Hannay, *Treatise on Solid State Chemistry*, Plenum Press, New York, 1921
13. D.C. Murray, N.L. Richards, and W.F. Caley, On Improving the Oxidation Resistance of a Ni-Based Superalloy Produced by Powder Metallurgy, *Can. Metall. Q.*, 2013, **52**, p 439–448
14. G. Baran, Oxidation Kinetics of Some Ni-Cr Alloys, *J. Dent. Res.*, 1983, **62**, p 51–55
15. J.M. Brossard, J. Balmain, F. Sanchette, and G. Bonnet, High-Temperature Oxidation of an Aluminized NiCr Alloy Formed by a Magnetron-Sputtered Al Diffusion Coating, *Oxid. Met.*, 2005, **64**, p 43–61
16. A. Ul-Hamid, Diverse Scaling Behavior of the Ni-20Cr Alloy, *Mater. Chem. Phys.*, 2003, **80**, p 135–142
17. G. Zeng, M. Li, J. Han, X. He, and W. Li, Oxidation Kinetics of Microcrystalline Ni-11.5Cr-4.5Co-0.5Al Superalloy Sheet Fabricated by Electron Beam Physical Vapor Deposition at 800 °C, *Mater. Lett.*, 2008, **62**, p 289–292
18. H.T. Mallikarjuna, N.L. Richards, and W.F. Caley, Isothermal Oxidation Comparison of Three Ni-Based Superalloys, *J. Mater. Eng. Perform.*, 2017, **26**, p 2014–2023
19. A. Akhtar, S. Hedge, and R.C. Reed, The Oxidation of Single-Crystal Nickel-Based Superalloys, *JOM*, 2006, **58**, p 37–42
20. S. Cruchley, H.E. Evans, M.P. Taylor, M.C. Hardy, and S. Stekovic, Chromia Layer Growth on a Ni-Based Superalloy: Sub-Parabolic Kinetics and the Role of Titanium, *Corros. Sci.*, 2013, **75**, p 58–66
21. C.S. Giggins and F.S. Pettit, Corrosion of Metals and Alloys in Mixed Gas Environments at Elevated Temperatures, *Oxid. Met.*, 1980, **14**, p 363–413
22. F.S. Pettit and G.H. Meier, Oxidation and Hot Corrosion of Superalloys, *Superalloys*, 1984, **85**, p 651–687
23. H.W. Liu and Y. Oshida, *Literature Survey on Oxidations and Fatigue Lives at Elevated Temperatures,* NASA Contractor Report 174639, Syracuse University, Syracuse, NY, USA, 1984
24. Y.G. Lai, *High-Temperature Corrosion and Materials Applications*, ASM International, Materials Park, 2007
25. M.W. Brumm and H.J. Grabke, The Oxidation Behaviour of NiAl-I. Phase Transformations in the Alumina Scale During Oxidation of NiAl and NiAl-Cr Alloys, *Corros. Sci.*, 1992, **33**, p 1677–1690
26. S.W. Yang, Effect of Ti and Ta on the Oxidation of a Complex Superalloy, *Oxid. Met.*, 1981, **15**, p 375–397
27. D.A. Akinlade, W.F. Caley, N.L. Richards, and M.C. Chaturvedi, Microstructural and Thermal Processing Effects on Adding 1 and 3 wt.% Ti to a Powder Metallurgy Processed Quaternary Ni-Cr-Fe-Al Alloy, *Mater. Sci. Eng. A*, 2011, **528**, p 996–1002
28. S. Taniguchi, T. Shibata, and H. Tsuruokat, Isothermal Oxidation Behavior of Ni_3AI-0.1B Base Alloys Containing Ti, Zr, or Hf Additions, *Oxid. Met.*, 1986, **26**, p 201–216
29. A. Naoumidis, H.A. Schulze, W. Jungen, and P. Lersch, Phase Studies in the Chromium-Manganese-Titanium Oxide System at Different Oxygen Partial Pressures, *J. Eur. Ceram. Soc.*, 1991, **7**, p 55–63
30. A.N. Blacklocks, A. Atkinson, R.J. Packer, S.L.P. Savin, and A.V. Chadwick, An XAS Study of the Defect Structure of Ti-Doped α-Cr_2O_3, *Solid State Ion.*, 2006, **177**, p 2939–2944
31. S. Cruchley, M.P. Taylor, H.E. Evans, M.C. Hardy, and D.J. Child, Characterisation of Subsurface Oxidation Damage in Ni Based Superalloy, RR1000, *Mater. Sci. Technol.*, 2014, **30**, p 1884–1889